

On galaxy spiral arms’ nature as revealed by rotation frequencies

Santi Roca-Fàbrega ¹, Octavio Valenzuela ², Francesca Figueras ¹, Mercè Romero-Gómez ¹, Héctor Velázquez ³, Teresa Antoja ⁴, Bárbara Pichardo ²

¹ *Departament d’Astronomia i Meteorologia and IEEC-UB, Institut de Ciències del Cosmos de la Universitat de Barcelona, Martí i Franquès, 1, E-08028 Barcelona.*

² *Instituto de Astronomía, Universidad Nacional Autónoma de México, A.P. 70-264, 04510, México, D.F.; Ciudad Universitaria, D.F., México.*

³ *Instituto de Astronomía, Universidad Nacional Autónoma de México, A. P. 877, 22800, Ensenada, México.*

⁴ *Kapteyn Astronomical Institute, University of Groningen, PO Box 800, 9700 AV, Groningen, The Netherlands.*

Accepted 2013 April 12. Received 2013 April 4; in original form 2013 February 27

ABSTRACT

High resolution N-body simulations using different codes and initial condition techniques reveal two different behaviours for the rotation frequency of transient spiral arms like structures. Whereas unbarred disks present spiral arms nearly corotating with disk particles, strong barred models (bulged or bulge-less) quickly develop a bar-spiral structure dominant in density, with a pattern speed almost constant in radius. As the bar strength decreases the arm departs from bar rigid rotation and behaves similar to the unbarred case. In strong barred models we detect in the frequency space other subdominant and slower modes at large radii, in agreement with previous studies, however we also detect them in the configuration space. We propose that the distinctive behaviour of the dominant spiral modes can be exploited in order to constraint the nature of Galactic spiral arms by the astrometric survey GAIA and by 2-D spectroscopic surveys like CALIFA and MANGA in external galaxies.

Key words: Galaxy: evolution — Galaxy: kinematics and dynamics — Galaxy: structure

1 INTRODUCTION

Since the early seventies, it has been suggested that the dynamics driven by bars and spirals have profound consequences on the kinematic and structural evolution of galactic disks (e.g. Miller et al. 1970; Hohl 1971; Athanassoula 1980; Sellwood & Athanassoula 1986; Friedli & Benz 1993). More recently, stellar radial migration in disk galaxies has been recognized as a critical component of disk galaxy evolution. This process may drastically alter our view of the connection between the present-day phase space and chemical distributions of stars and the processes of disk formation and evolution. Sellwood & Binney (2002) set up the dynamical framework of this process through the effects of transient spiral structure, which seems to be a crucial process to understand the solar neighborhood observations as suggested originally by Wielen et al. (1996). Authors such Roskar et al. (2008), Schönrich & Binney (2009), Roskar et al. (2011) and Minchev et al. (2012), among others, revived the study of spiral arms and bars as triggers of stellar radial migration. Despite these numerous studies, fundamental questions arise such as: what is the nature of the spirals? or, how is their pattern speed related to the motion of the stellar component? Several models have been proposed up to now, from the classical Tight-Winding Approximation (TWA, e.g. Binney & Tremaine 2008) to the mechanisms proposed to account for self-excited spiral patterns (Toomre 1990; Bertin & Lin 1996;

Sellwood 2000; D’Onghia et al. 2013), or the manifold theory (Romero-Gómez et al. 2007; Tsoutsis et al. 2009; Athanassoula 2012).

In the quest of dynamical models not limited to quasilinear approximations or steady state, N-body simulations have been used to understand the origin and evolution of spiral structures. After pioneering studies like Miller & Smith (1979); Sellwood & Sparke (1988); Rautiainen & Salo (1999), only recently appeared another boom of papers likely as a result of progress in the computational resources and codes. This re-ignition of simulations based studies opened-up an interesting debate about the possible corotating nature of spiral patterns with disk particles (e.g. Quillen et al. 2011; Grand et al. 2012a,b; Minchev et al. 2012; D’Onghia et al. 2013; Baba et al. 2013). As an example, Grand et al. (2012a,b) computed collisionless N-body and smoothed particle hydrodynamics (SPH) simulations of disk galaxies and illustrated that transient spiral features appear to corotate with the disk. Comparetta & Quillen (2012) also suggested that some short lived features arising from constructive interference between longer lived modes, i.e. fast bar and slowly moving spiral pattern modes, can be nearly corotating with the disk. This corotating nature would have consequences on the stellar radial migration mechanisms (Grand et al. 2012a).

From the observational point of view, the nature of spiral arms is also far from being clear (Sheth & Rossi 2010; Foyle et al. 2011; Ferreras et al. 2012). Nowadays, only weak observational con-

straints are available to answer these questions. Some constraints come out from direct measurement of the rotation frequencies radial variation in external galaxies (e.g. Meidt et al. 2009), a method with a strong potential but currently applied only to a handful of galaxies, or from indirect measurements as the one proposed by Martínez-García et al. (2009). Other constraints to spiral arms' nature are based on small scale stellar kinematic substructure analysis in the Milky Way (MW) disk (e.g. Antoja et al. 2011, 2012). Furthermore, although it is now commonly accepted that the MW is a barred galaxy, it is not clear how the arms and bar are related or if they are connected at all. The rotation frequency of both, bar and spiral arms, seem to show different values, none in mutual corotation or in corotation with galactic disk material, leaving unclear spiral arms' nature (Martos et al. 2004; Gerhard 2011). It is fair to say that currently, galactic arms' pattern speed estimations are mostly model dependent (Martos et al. 2004). The situation is also not clear for external galaxies (Buta et al. 2005). The interpretation of observational results is based on previous theoretical studies and also on numerical simulations (Sellwood & Sparke 1988; Rautiainen & Salo 1999). Some of these studies adopted simplifications like 2D N-body models and a rigid halo or no halo at all. It is not clear if such assumptions may affect the generality of their conclusions as is suggested by Athanassoula (2002) for the case of bar growth. It is also not obvious if the corotating nature of spiral arms recently suggested by Grand et al. (2012a) is valid also in models with different structure (i.e. models with strong/weak bar and/or bulge). Furthermore, classical methods to estimate disk modes' rotation frequencies like time Fourier spectrograms applied to simulations, have been claimed to suffer from biases in models with multiple or weak spiral arms, hampering estimations of arms' pattern speeds (Grand et al. 2012a).

In this paper we analyze 3D galaxy models, with different stellar/dark structure, using live halos and with enough mass, force and time resolutions to accurately describe the internal disk kinematics. We performed some testing on the results dependence on codes and initial conditions techniques. It should be emphasized that the N-body simulations presented here are purely stellar. From the first attempts to simulate gas in barred galaxies (Sanders & Huntley 1976), it has become clear that gas influences disk stellar dynamics, by even changing the live time of bars (Bird et al. 2012; Di Matteo et al. 2013). Gas makes disks to show more complicated and well-defined morphologies. As an example, inner rings, such the Galactic Molecular Ring observed in our MW (Clemens et al. 1988), have been the subject of numerous observational (Buta et al. 2004) and theoretical investigations (e.g. Byrd et al. 2006; Romero-Gómez et al. 2011). The influence of the gaseous component and its subgrid physics in our simulations is now under investigation using the ART code in the hydrodynamic version (Kravtsov 2003; Colín et al. 2010).

The aim of the first study presented here is to revisit the possible correlation between spiral arm kinematics and their nature using the purely stellar component. In Section 2 we describe our N-body simulations, carried out using two well known N-body codes, ART and GADGET3. In Section 3, we describe the techniques used to derive the rotation frequencies, whereas the results and conclusions are presented in Section 4 and 5, respectively.

2 MODELS AND SIMULATIONS

We have performed collisionless N-body simulations with ART (Kravtsov et al. 1997) and GADGET3 (last described in Springel

Parameter	B1/5	G1	U1/5
Disk mass ($10^{10} M_{\odot}$)	5.0	6.01	3.75
Halo mass ($10^{12} M_{\odot}$)	1.38	0.66	1.5
Disk exp. length R_d (kpc)	3.86	3.0	4.0
Disk exp. height Z_d (kpc)	0.2	0.2	0.2
Halo NFW R_d (kpc)	29.19	14.4	16.61
Halo concentration	10	10.4	18
Halo DM species	6/7	1	6/7
$N_{*disk} (+N_{*bulge}) (10^6)$	1.0/5.0	0.5(+0.5)	1.0/5.0
$N_{eff} (10^7)$	2.86/13.8	0.15	4.1/20.0
Min. time step (10^4 yr)	3.2/1.6	4.4	7.9/3.1
Spatial Resolution (pc)	44.0/11.0	35.0	11.0/11.0
Total integration t (Gyr)	4.6/2.8	1.4	3.2/2.8

Table 1. Parameters of the simulations: Column indicated by B1/5 presents the parameters for models with 1 million (B1) and 5 million (B5) star particles in the disk, simulated using ART code, idem for unbarred models U1/5 in the third column and for the barred model G1, using GADGET3 code, in the second column.

2005) codes. Tests of consistency of both codes, applied to dynamics of barred galaxies can be found in Valenzuela & Klypin (2003), Colín et al. (2006) and in Klypin et al. (2009). We present here three sets of fully self-consistent models, all of them with a live exponential disk and live dark matter halo with the NFW (Navarro et al. 1997) density profile (see Table 1). The live halo ensures disk-halo angular momentum exchange, which plays an important role in the formation and evolution of bars as discussed by Athanassoula (2002). We simulated barred (B) and unbarred (U) models with the aim to compare spiral arms potentially triggered by a bar against arms triggered by other mechanisms. Models B and U were simulated using the ART code. To generate initial conditions of these models we used the Jeans equation moments method as introduced by Hernquist (1993). We have also used a multimass method to sample the halo particle distribution, which allows us to obtain similar results as using a higher number (N_{eff}) of particles, minimizing two body scattering as discussed in Valenzuela & Klypin (2003). Barred models have a stellar disk and total mass similar to the one observed for the MW with additional initial parameters as proposed by Colín et al. (2006) (model K_{cb}). As discussed in (Klypin et al. 2002), the final properties of this model, after rescaling, can reproduce the observed quantities for the MW. This rescaling process has not been applied since it does not affect the disk kinematic properties analysed in this paper. Unbarred models have a smaller disk and a massive and highly concentrated halo. Additionally we have used the GADGET3 code to simulate barred models, labeled G, including a bulge component with a Sersic profile ($R_b = 1.75$ kpc, $M_b = 8.57 \cdot 10^9 M_{\odot}$). For the bulged models' initial conditions generation we have used the code described in Widrow & Dubinski (2005). The number of disk particles in our models range from one to five million particles (see Table 1).

As expected (e.g. Ostriker & Peebles 1973), the models with a relatively dominant disk (B and G) rapidly generate a bar with trailing spiral arms while unbarred models (U) do not, at least in

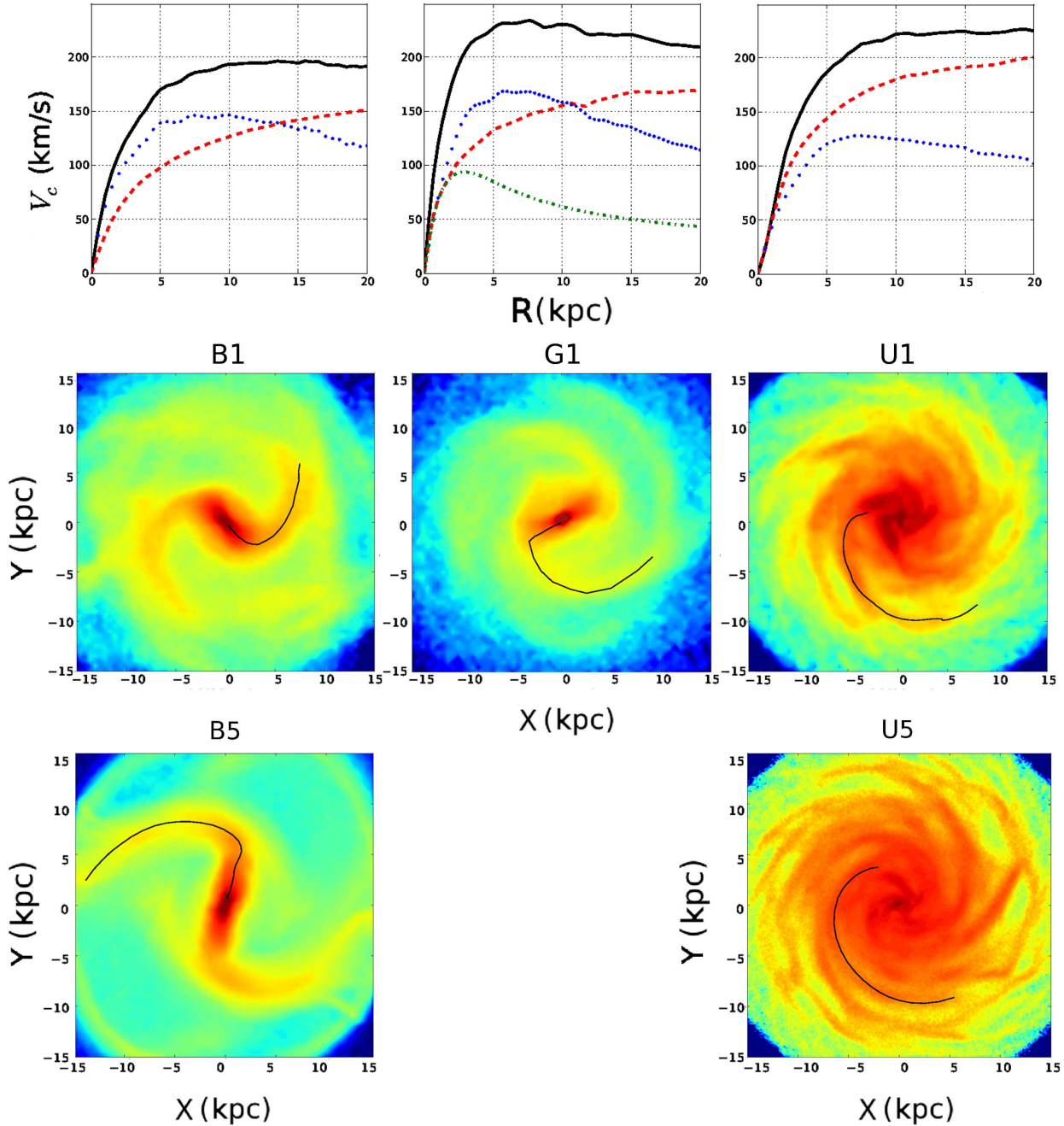


Figure 1. Structure of the models. Top: Initial circular velocity of models B (left), G (center) and U (right), computed from the potential field gradients using TIPSy package. We show the total rotation curve (black solid), disk (blue dotted), halo (red dashed) and bulge (green dot-dashed) contributions. Center: Density distribution of the models B1 (left), G1 (center) and U1 (right) after 900 Myr of evolution. Bottom: Density distribution of the models B5 (left) and U5 (right) after 900 Myr of evolution. The black solid line shows the locus of the spiral arms derived using Fourier analysis ($m = 2$ for B and G models, $m = 4$ for U). Spiral structure rotates clockwise in all models.

the first ~ 3 Gyrs. In the first case, we have a similar halo and disk contribution to the circular velocity inside a radial exponential length and, as described in Valenzuela & Klypin (2003), the self-gravity of disk density fluctuations (disk modes) dominates making the instability grow and generate a bar (Figure 1, left and middle panels). This bar mode induces the formation of a

bisymmetric spiral structure apparently connected to the bar ends (e.g. Binney & Tremaine 2008, and references therein). There is still controversy on the nature of these bisymmetric spirals (resonant coupling, manifolds, or others), but what is evident in all our models is that these structure dominates in density. For the unbarred model (Figure 1, right) the halo contribution

to the potential is higher and the disk modes cannot grow so easily. Although in both cases the initial velocity dispersion is low ($Q = 1.2$), the higher halo mass concentration in the unbarred model prevents disk from having a dominant bisymmetric mode in the first Gyrs of evolution, i.e. other modes grow forming a trailing 3-4 armed structure. Some other structures with lower density appear in the external regions of these simulations (both barred and unbarred). In the next section we discuss their imprints on the frequency space. As expected for MW like galaxies, we also note that rotation curves in our set of simulations are rather flat (see top panels of Figure 1).

In all our models spiral arm structures are observed for at least 2-3 Gyrs. We show in Figure 2 the temporal evolution of the spatial Fourier modes for the three models with one million particles in the disk. We see that dominant spiral modes have a recurrent nature with periodicities of less than one galactic rotation. The amplitude of the spiral arms in the unbarred case is significantly lower than in the barred models.

In Figure 1 we observe that some parameters of the bar and spirals are different from B1 (one million disk particles) to B5 (five million) models. These differences are arising from the fact that the number of particles, spatial and time resolution in B5 model are much better than in B1, i.e. we are resolving smaller wavelength disk modes in the B5 case than in B1. These modes interact with the disk and then, due to the high non-linearity of the system, lead the evolution to a slightly different configuration (e.g. bar length and speed). However global quantities like circular velocity and density profiles are more robust to such effects. The situation is well known and it has been reported in previous works (Sellwood & Debattista 2009; Klypin et al. 2009). A convergence study of this and other models will be presented in Roca-Fàbrega et al. (in preparation), however, as will be seen in next sections, the main results of our simulations are robust across changes in numerical parameters: a bar-arm structure which is dominant in density plus external and weaker arms are formed in barred disks, while in barless models low amplitude arms are found. In the next section we will analyse the kinematics of such spirals structures.

3 OVERDENSITIES AND ROTATION FREQUENCIES

We use spatial Fourier analysis azimuthally averaged in order to trace the density peak of the spirals and the bar (Valenzuela & Klypin 2003), working in cylindrical shells equally spaced in galactocentric distance. Figure 1 shows an example of how well the spatial Fourier method traces the peak overdensities up to the end of the dominant structures ($m=2$ for barred cases and $m=3,4$ for unbarred ones). We also used a density peak method as the one used in Grand et al. (2012a,b) to test that the results are method independent. Once the locus of the spiral is derived, we use both, finite differentiation among three consecutive snapshots and the classical spectrograms method (Sellwood & Athanassoula 1986) to compute the rotation frequency.

The advantages of using Spatial Fourier plus Finite Differentiation (hereafter SFpFD) are that it allows us to compute the rotation frequency of a single known mode m structure and for a single time instant. As a consequence, SFpFD is able to show us how the structures evolve with time. On the contrary the spectrogram method (Sellwood & Athanassoula 1986) needs to be applied to a large time interval due to the Nyquist frequency limitation. Because of that, the results from spectrograms method may be

contaminated by recurrent arms sequences with low or negligible spiral amplitude due to the transient nature of the structures. This drawback is already discussed by Grand et al. (2012a).

A weakness of using SFpFD, independently of having two or more spiral arms, appears when two coexisting structures of the same Fourier mode at the same radius are present. In this case, the method results in an unique structure placed at the average angle. Thus, we have to control these cases to avoid a bias in the derived rotation frequency. In contrast spectrograms can find discrete rotation frequencies from structures coexisting at the same radius without any problem. After carefully weighting the pros and cons we state that both methods (SFpFD and spectrograms) are complementary.

4 SPIRAL ARM ROTATION FREQUENCIES

We perform a first kinematical analysis on the dominant modes in density shown in Figure 2, $m = 2$ for the barred (bisymmetric spiral) and $m = 4$ for the unbarred models (4 armed structure). As can be seen in Figure 1, the dominant density structures extend up to 10 – 11 kpc. In Figure 3 we present the rotation frequency curves for the three models with one million disk particles computed using the SFpFD method. It includes all timesteps where we can ensure the spiral arm is well formed. We empirically establish that a spiral is well formed when the amplitude of the dominant mode is above 0.7 times the maximum value of this mode in the range we study (see thin black dashed lines in Figure 2). These density maps are constructed from the superposition of all the rotation frequency curves at timesteps when the amplitude of the mode is above the mentioned threshold. These figures show significant differences between barred and unbarred morphologies. Note how in the barred models (B1 and G1, computed using ART and GADGET3, respectively) the spiral pattern rotates almost as a rigid body, while in unbarred models the rotation frequency curves lie on top of the rotation of the disk particles, resulting in a spiral mode corotating with the disk.

A more exhaustive analysis is shown in Figure 4, considering models with a higher number of disk particles and a different technique for the detection of the spiral structure. Instead of working with density maps, here we plot single timestep curves computed using SFpFD for models with both one and five million disk particles. For the B and G models we avoid the central part of the bar, for U the central complex region where the 3-4 armed structure converges and in both we also avoid the external regions where the number of particles is too low. The red-dashed lines correspond to two instants of the one million disk particle models (included in the density plot of Figure 3) shown as red dots in Figure 2. More important, the blue-dashed lines correspond to models with five million disk particles, both barred and unbarred, integrated using ART. Furthermore, the blue-dotted line corresponds to the barred ART five million model for which the spirals have been detected using the density peak method (similar to the one in Grand et al. (2012a,b)). Note how the conclusions reached in Figure 3 are well corroborated. We can see spiral patterns rotating almost as a rigid body in all our barred models, both using ART and GADGET3, using different techniques for the spatial detection and considering a different number of particles. We have also verified that simulations with $2 \cdot 10^5$ disk particles show the same behaviour (not included here). A slightly decreasing rotation frequency with radius is observed only for the ART model with one million disk

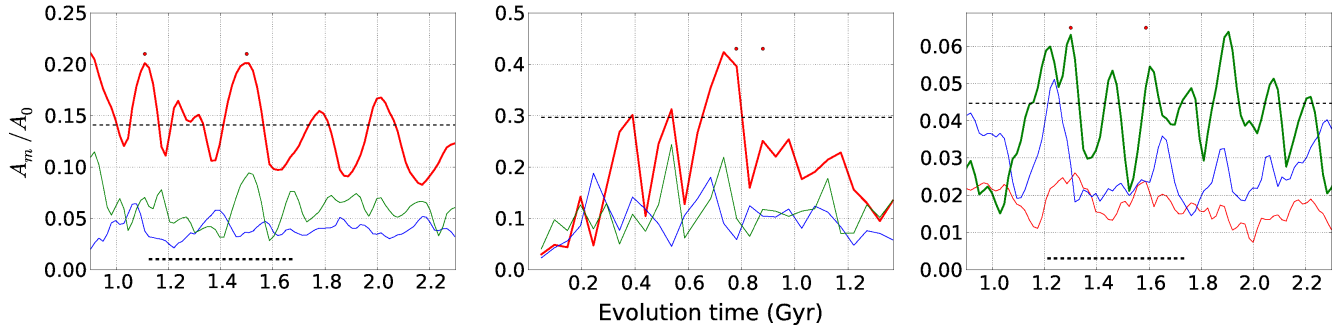


Figure 2. Amplitude evolution of disk modes. Fourier amplitude for modes 2 (red), 3 (blue) and 4 (green) as a function of time, averaged for radius between 4 and 10kpc of the barred (B1, left), the bulge-barred (G1, center) and the unbarred (U1, right) models (notice change in vertical scale). Thin black dashed lines indicate a threshold in amplitude used to compute Figure 3 using SFpFD method. The black dots indicate the snapshots for which the kinematic analysis is shown in Figure 4 using SFpFD method, and thick black dashed lines indicate the temporal range used to compute spectrograms in Figure 5.

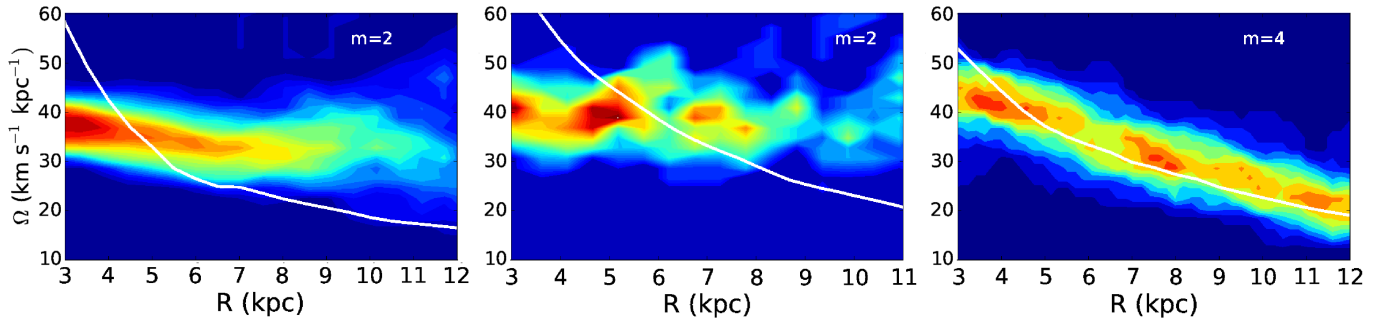


Figure 3. Rotation frequencies as a function of radius calculated using SFpFD method for dominant mode across time in models B1 (left), G1 (center) and U1 (right) (see Figure 2). Here we plot the frequency density map of the rotation frequencies computed using all time instants when the spiral arms' amplitude is above 70% of the maximum mode amplitude (dashed line in Figure 2). Circular frequencies of disk particles are indicated as solid white lines and have been computed in an intermediate instant of the analyzed time interval. The length of the bar is ~ 4.5 kpc and ~ 5 kpc for B1 and G1 models respectively.

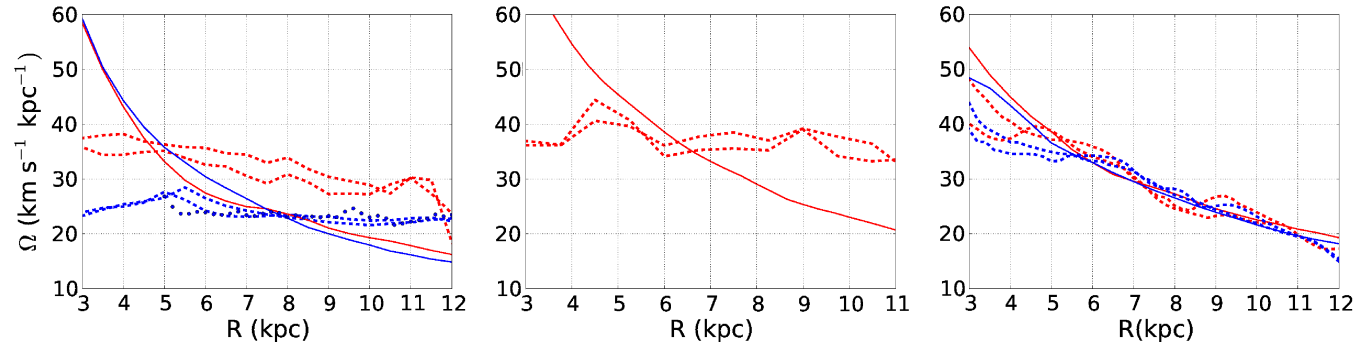


Figure 4. Rotation frequencies as a function of radius calculated using SFpFD method for selected time instants when the amplitude of spiral arms is maximum (black dots in Figure 2). All the rotation frequencies analysis of barred (B1, and B5 left), the bulge-barred (G1, center) and the unbarred (U1, right) has been computed taking cylindrical shells of 0.5kpc width. In red dashed we show results obtained for models with 1 million disk particles. In blue dashed, those of the ART models, with 5 million disk particles (left and right panels respectively, for models B5 and U5) when the amplitude of the spirals arms is maximum (0.75 and 1.12 Gyr). Circular frequencies of disk particles are indicated as solid lines (red for models B1 and U1 and blue models B5 and U5). Additionally, blue dots in the left panel show the results of applying a density peak method similar to one used in Grand et al. (2012a) to B5 simulation, to find the spiral structure (a detailed description of this method will be included in Roca-Fàbrega et al. in preparation). The dispersion on rotation frequency profiles due to its computation at several time steps when the amplitude of the dominant mode and its behaviour can slightly change, is shown at Figure 3. The length of the bar is ~ 4.5 kpc, ~ 7.0 kpc and ~ 5.0 kpc for B1, B4 and G1 models respectively. The differences in bar properties between models B1 and B5 are discussed in Section 2.

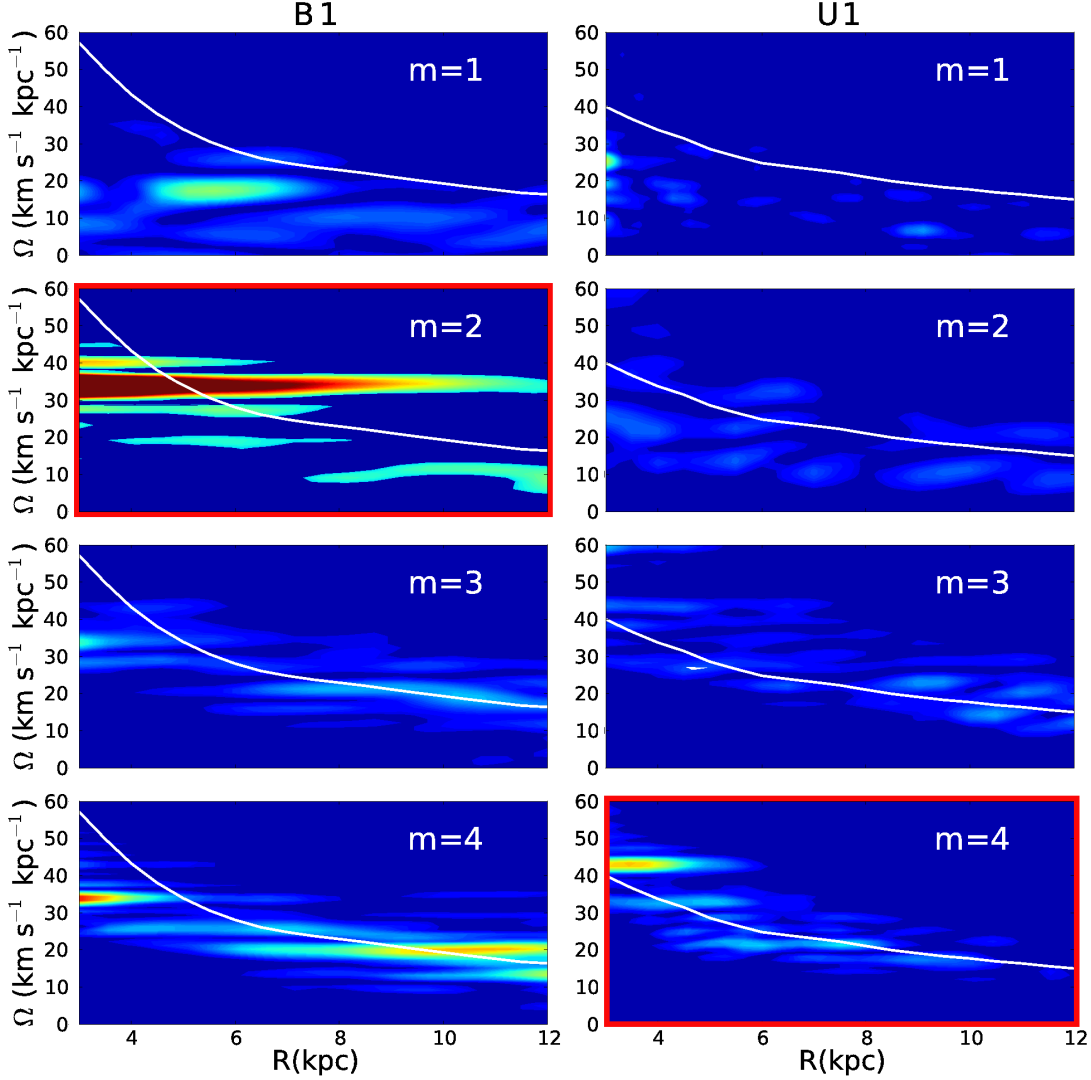


Figure 5. Spectrograms for the barred model B1 (left) and unbarred U1 (right) obtained using Sellwood & Athanassoula (1986) method. We show the Fourier component for the $m=1,2,3$ and 4 modes in a window spanning 0.5 Gyr centered at 1.4 Gyr (left) and 1.45 Gyr (right), (see dashed dark lines in top panels of Figure 2), and with a Nyquist frequency $\sim 100 - 150 \text{ km s}^{-1} \text{ kpc}^{-1}$. The y axis is the angular frequency in $\text{km s}^{-1} \text{ kpc}^{-1}$ and the x axis is radius in kpc. Overplotted in white we show the rotation curve of disk particles computed for an intermediate instant of the analyzed time interval.

particles (B1). Even though, this behaviour is completely different from all our ART unbarred models, both using one million and five million disk particles.

To ensure that our results are not dependent of the method used to compute the rotation frequencies, in Figure 5, we perform one last test using, in this case, the classical spectrogram method in B1 and U1 models with a Nyquist frequency of $\sim 100 - 150 \text{ km s}^{-1} \text{ kpc}^{-1}$. The panels framed in red correspond to the dominant modes discussed above, and they are to compare with the left and right panels of Figure 3. Note that, again, the barred model presents a dominant mode that rotates as a rigid body, while in the unbarred case, the structures corotate with the disk particles. Two features observed in this dominant modes deserve special attention. First, in the barred model, a well defined structure is observed at a radial range of $11 - 14 \text{ kpc}$ (only the beginning of the structure is shown in the figure). It rotates slower than the disk with a frequency of about $8 \text{ km s}^{-1} \text{ kpc}^{-1}$. As mentioned in

Section 3, here we note one of the advantages of the spectrograms. They are able to detect multiple spiral patterns at a given radius. Using SFpFD, we have checked that the low frequency structure corresponds to one of the lower density structures observed in the outer radii of the center-left panel of Figure 1. The complex link with the dominant structure will be discussed in a forthcoming paper. As it is known, these multiple pattern speeds are common in spiral barred galaxies both in simulations and observations (e.g. Masset & Tagger 1997; Buta & Shang 2011). Secondly, and less important, we can appreciate a flat structure in the rotation frequency in the central region of the unbarred model ($R < 4 \text{ kpc}$, bottom right panel of Figure 5), which could remind the signature of a weak bar mode. This is a misinterpretation since it corresponds to a $m = 4$ mode, and, actually, the amplitude of the $m = 2$ mode in this region is less than 2% (see Figure 2).

Figure 5 also includes the spectrograms for the subdominant modes. As in Figure 6 of Grand et al. (2012a) we find all these

subdominant modes clearly corotating with the disk. This behaviour is also observed in other studies as in Minchev et al. (2012) (Figure 8), although not discussed there, while they are centered on the study of resonant coupling.

5 DISCUSSION AND CONCLUSIONS

The rotation frequencies of the spiral modes in barred and unbarred models, integrated with different N-body codes (ART and GADGET), and analysed with different techniques (spectrograms and finite differences), present a well defined different behaviour. Whereas unbarred models show transient arms corotating with disk particles, in good agreement with those recently reported by Grand et al. (2012a) and Baba et al. (2013), barred models deserve further comments. As shown in Figures 3 and 4, barred models present a spiral pattern speed almost constant in radius for all the range where the spiral structure is dominant in density. These results are consistent with those of models I, II and III in Rautiainen & Salo (1999), computed using a simplified 2D model and with rigid or no halo. We want to emphasize that whereas in those early models it is difficult to detect spiral structures in the configuration space, particularly in the external regions, in our simulations with 1 and 5 million disk particles, the spiral structure is clearly identified (see Figure 1), allowing us to use the arm phase in order to test claimed biases in the derivation of the rotation frequencies using spectrograms (see Section 3).

It is important to compare our results with those recently obtained by Grand et al. (2012b). The authors have analyzed N-body/SPH simulations of isolated barred galaxies concluding that, spiral arms' pattern speed decreases with radius, closely in corotation with disk particles. Grand et al. (2012b) computed the rotation frequencies averaging the values obtained for several snapshots over two time intervals during spiral arm evolution, one when the bar is well defined in their images (~ 1 Gyr of evolution, see their Figure 9) and the other when the bar has significantly weakened (~ 1.5 Gyr, Figure 10). In both cases, the spirals pattern speed is almost corotating with disk particles. The previous result is at odds to what is obtained in our study. However they also noticed a small offset of the spiral arms' rotation frequency profile from being corotating with disk particles, particularly when the bar is stronger, suggesting that further analysis is required. Here we have analyzed the correlation between the strength of the bar and the spiral rotation frequency in our B1 ART model, a Milky Way like simulation. With such a purpose, we have computed arms' rotation frequency during the first evolutionary stages, when the bar is still growing and weak ($A_2/A_0 < 0.1$) at about 0.3 Gyr of evolution. Only when the bar is weak we observe that the external $m=2$ mode (bisymmetric arm) rotation frequency is close to disk corotation. After few galactic rotations, when the bar has fully formed ($A_2/A_0 > 0.4$) (as shown in Figure 2 left panel), the rotation frequency becomes almost constant, approaching the bar rigid body rotation, if any with a small decrement in radius (see Figure 3 and 4, left and central panels). This result is qualitative in agreement with the statement discussed by Grand et al. (2012b), unfortunately we do not have information of bar amplitude in Grand et al. (2012b) simulations, and their models assume a gas component making harder a further comparison. We conclude that in barred models the spiral rotation frequency approaches the bar rigid body rotation with the increment of bar strength. Furthermore, our simulations, with a high number of disk particles,

allow us to analyze the behaviour at larger radii $\sim 12 - 14$ kpc. As can be seen in Figure 5 ($m=2$ mode, left panel second row), the spectrograms method applied to the B1 bar model shows an external structure, at radii larger than $R=11$ kpc, that rotates slower than the density dominant mode. This external structure has a lower amplitude, lower rotation frequency (less than $10 \text{ km s}^{-1} \text{ kpc}^{-1}$), it is tightly wound, and it is recurrently connected/disconnected with the inner and faster spiral (see movie¹). Other authors (i.e Sellwood & Sparke 1988) have reported similar structures but apparently they detected them only in the frequency space, probably due to the statistical fluctuations given by their number of particles (see however figure 16 in Rautiainen & Salo (1999)). The lack of detection in configuration space led the authors to conclude that inner fast rotating structures correspond only to the bar structures while the slower and external ones to the entire and unique spiral mode. Here we confirm the detection and the rotation frequency in configuration space (see Figure 1) for all these structures, and that the inner fast rotating structure includes both: a bar and an inner spiral structure apparently connected. The slow rotating mode is an external spiral mode. We stress that we also find both structures using the SFpFD method in configuration space. In conclusion, at large radii, and for $m=2$, we do see the external slow and low amplitude arm coexisting with the dominant spiral mode which is most of the time connected to the bar.

The results presented here for the barred case are also compatible with the observations recently reported by Meidt et al. (2009). They derive rotation frequencies in four spiral galaxies: two strong barred, one unbarred and one with rings. They find that in the two strong barred cases the inner bisymmetric spirals rotate with the same frequency as the bar. Furthermore, one of the barred cases present an external armed structure rotating with a much lower frequency (see their Figures 8 and 12) as it is observed in our B1 barred model. For the other cases they find multiple pattern speeds that can be or not in a resonance coupling situation. It is important to mention that at least one of their barred galaxies is likely in interaction (M101). As discussed by the authors, the limiting observational accuracy - precision in the radial binning and frequency sampling - do not allow them to confirm or refute the small radial decrement in rotation frequency shown in our Figure 3, therefore they conclude that arms in their study are rigid body rotators. Further observations will be required to confirm this tendency.

From the simulations we have performed it is clear that a difference in the spiral arm kinematics exists if they are triggered by a bar or by another mechanism, and also that barred models seem to show at least two kinds of spiral arms. Further analysis of the arm nature, and numerical convergence tests will be discussed in a forthcoming paper.

As a summary we confirm that:

- The dominant spiral mode ($m=2$) in strong barred models is most of the time connected to the bar. Its rotation frequency is near to the bar solid body rotation, with a small decrement with radius which is more important as the bar amplitude decreases. Arms are corotating with disk particles only for very weak bars.

¹ This movie can be downloaded from <http://www.am.ub.edu/~sroca/Nbody/movies/B1.mpeg> and it shows the density evolution of model B1, spanning from 0.1 to 3.1 Gyrs. High density regions ($\sim 3.7 \text{ M}_\odot/\text{pc}^3$) are shown in dark-blue colors while zero density ones are in white.

- Although the dominant spiral disk mode in barred simulations is the one connected with the bar, we observe at least one subdominant slow and winded mode at large radii, using either SFpFD, spectrograms (see Figure 5) and density maps.

- In unbarred models the spiral structures are corotating with disk material, in agreement with previous results Grand et al. (2012a).

- Our results are robust to changes in numerical parameters (time step, spatial resolution, number of particles), mode analysis techniques (SFpFD, spectrograms, density peak) and also to changes in numerical codes (ART and GADGET3).

A natural question is to ask which is the situation for the MW: Do the traditional spiral arms correspond to the mode coupled with the bar? or instead correspond to the modes we observed at larger radii? or both? Planned and current surveys measuring stellar kinematics and distances inside our Galaxy as Gaia (ESA) or APOGEE (SDSS) will open up the possibility of direct estimation through methods like the one proposed by Tremaine & Weinberg (1984). Spectroscopic high resolution surveys of external galaxies like CALIFA (Sánchez et al. 2012) or MANGA(AS3/SDSSIV) will contribute to test our predictions using stellar kinematics.

We thank A. Klypin, A. Kravtsov and V. Springel for providing us the numerical codes and L. M. Widrow for providing the code to generate the initial conditions. We thank HPCC project and T. Quinn for the implementation of TIPSy package. Finally we also thank Luis Aguilar, Ivanio Puerari and Gene G. Byrd for his helpful comments on this work. This work was supported by the MINECO (Spanish Ministry of Economy) - FEDER through grant AYA2009-14648-C02-01, AYA2010-12176-E, AYA2012-39551-C02-01 and CONSOLIDER CSD2007-00050. SR was supported by the MEC D PhD grant 2009FPU AP-2009-1636. Simulations were carried out using Pakal, Abassi2 and Atocatl at IA-UNAM, and Pirineus at CESCA.

REFERENCES

- Antoja T., Figueras F., Romero-Gómez M., Pichardo B., Valenzuela O., Moreno E., 2011, *MNRAS*, 418, 1423
- Antoja T., Helmi H., Bienayme O., et al. 2012, *MNRAS*, 426, L1
- Athanassoula E., 1980, *A&A*, 88, 184
- Athanassoula E., 2002, *ApJ*, 569, L83
- Athanassoula E., 2012, *MNRAS*, 426, L46
- Baba J., Saitoh T. R., Wada K., 2013, *ApJ*, 763, 14
- Bertin G., Lin C. C., 1996, Cambridge, MA MIT Press
- Binney J., Tremaine S., 2008, *Galactic Dynamics*, 2nd edn. Princeton Univ. Press, Princeton, NJ
- Bird J. C., Kazantzidis S., Weinberg D. H., 2012, *MNRAS*, 420, 913
- Buta R. J., Byrd G., Freeman T., 2004, *AJ*, 127, 1982
- Buta R. J., Laurikainen E., Salo H., Block D. L., Knapen J. H. R., 2005, *AAS*, 37, 1481
- Buta R. J., Shang X., 2011, *MSAIS*, 18, 13
- Byrd R., Freeman T., Buta R. J., 2006, *AJ*, 131, 1377
- Clemens D. P., Sanders D. B., Scoville N. Z., 1988, *ApJ*, 327, 139
- Colín P., Avila-Reese V., Vázquez-Semadeni E., Valenzuela O., Ceverino D., 2010, *ApJ*, 713, 535
- Colín P., Valenzuela O., Klypin A., 2006, *ApJ*, 644, 687
- Comparetta J., Quillen A. C., 2012, *ArXiv e-prints* (arXiv:1207.5753)
- Di Matteo P., Haywood M., Combes F., Semelin B., Snaith O. N., 2013, *ArXiv e-prints* (arXiv:1301.2545)
- D’Onghia E., Vogelsberger M., Hernquist L., 2013, *ApJ*, 766, 14
- Ferreras I., Cropper M., Kawata D., Page M. Erik A., 2012, *MNRAS*, 424, 1636
- Foyle K., Rix H. W., Doobs C. L., Leroy A. K., Walter F., 2011, *ApJ*, 735, 101
- Friedli D., Benz W., 1993, *A&A*, 268, 65
- Gerhard ., 2011, *MSAIS*, 18, 185
- Grand R. J. J., Kawata D., Cropper M., 2012a, *MNRAS*, 426, 167
- Grand R. J. J., Kawata D., Cropper M., 2012b, *MNRAS*, 421, 1529
- Hernquist L., 1993, *ApJS*, 86, 389
- Hohl F., 1971, *ApJ*, 168, 343
- Klypin A. A., Valenzuela O., Colín P., Quinn T., 2009, *MNRAS*, 398, 1027
- Klypin A. A., Zhao H., Somerville R. S., 2002, *ApJ*, 573, 597
- Kravtsov A. V., 2003, *ApJ*, 590, L1
- Kravtsov A. V., Klypin A. A., Khokhlov A. M., 1997, *ApJS*, 111, 73
- Martínez-García E. E., González-Lópezlira R. A., Bruzual G., 2009, *ApJ*, 694, 512
- Martos M., Hernández X., Yáñez M., Moreno E., Pichardo B., 2004, *MNRAS*, 350, 47
- Masset F., Tagger M., 1997, *A&A*, 322, 442
- Meidt S. E., Rand R. J., Merrifield M. R., 2009, *ApJ*, 702, 277
- Miller R. H., Prendergast K. H., Quirk W. J., 1970, *ApJ*, 161, 903
- Miller R. H., Smith B. F., 1979, *ApJ*, 227, 785
- Minchev I., Famaey B., Quillen A. C., Di Matteo P., Combes F., Vlajić M., Erwin P., Bland-Hawthorn J., 2012, *A&A*, 548, 126
- Navarro J. F., Frenk C. S., White S. D. M., 1997, *ApJ*, 490, 493
- Ostriker J. P., Peebles P. J. E., 1973, *ApJ*, 186, 467
- Quillen A. C., Dougherty J., Bagley M. B., Minchev I., Comparetta J., 2011, *MNRAS*, 417, 762
- Rautiainen P., Salo H., 1999, *A&A*, 348, 737
- Romero-Gómez M., Athanassoula E., Antoja T., Figueras F., 2011, *MNRAS*, 418, 1176
- Romero-Gómez M., Athanassoula E., Masdemont J. J., García-Gómez C., 2007, *A&A*, 472, 63
- Roskar R., Debattista V. P., Loebman S. R., Ivezić Z., Quinn T. R., 2011, *ASPC*, 448, 371
- Roskar R., Debattista V. P., Quinn T. R., Stinson G. S., Wadsley J., 2008, *ApJ*, 684, 79
- Sánchez S. F., Kennicutt R. C., Gil de Paz A., et al. 2012, *A&A*, 538, A8
- Sanders R. H., Huntley J. M., 1976, *ApJ*, 209, 53
- Schönrich R., Binney J., 2009, *MNRAS*, 396, 203
- Sellwood J. A., 2000, *Ap&SS*, 272, 31
- Sellwood J. A., Athanassoula E., 1986, *MNRAS*, 221, 195
- Sellwood J. A., Binney J. J., 2002, *MNRAS*, 336, 785
- Sellwood J. A., Debattista V. P., 2009, *MNRAS*, 398, 1279
- Sellwood J. A., Sparke L. S., 1988, *MNRAS*, 231, 25
- Sheth R. K., Rossi G., 2010, *MNRAS*, 403, 2137
- Springel V., 2005, *MNRAS*, 364, 1105
- Toomre A., 1990, *International Conference on Dynamics and Interactions of Galaxies*, p. 292
- Tremaine S., Weinberg M. D., 1984, *ApJ*, 282, 5
- Tsoutsis P., Kalapotharakos C., Efthymiopoulos C., Contopoulos G., 2009, *A&A*, 495, 743
- Valenzuela O., Klypin A. A., 2003, *MNRAS*, 345, 406
- Widrow L. M., Dubinski J., 2005, *ApJ*, 631, 838
- Wielen R., Fuchs B., Dettbarn C., 1996, *A&A*, 314, 438

This paper has been typeset from a $\text{T}_{\text{E}}\text{X}/\text{L}^{\text{A}}\text{T}_{\text{E}}\text{X}$ file prepared by the author.